Observation of electron two-dimensional standing-wave patterns at the surface of an insulating layer by scanning tunneling microscopy

Thibault Ardhuin,[1] Olivier Guillermet,[1] Carlos Javier Villagómez,[2] André Gourdon,[1] and Sébastien Gauthier[1]
[1]*CEMES CNRS UPR 8011 and Université de Toulouse, 29 rue Jeanne Marvig, 31055 Toulouse, France*
[2]*Instituto de Física, Universidad Nacional Autónoma de México, Apartado Postal 20–364, 01000 CDMX, México*

(Received 9 August 2018; revised manuscript received 29 November 2018; published 7 January 2019)

Electron standing wave patterns around single hexa-*peri*-hexabenzocoronene (HBC) molecules adsorbed on the surface of thin KBr(001) films grown on Ag(111) are observed by scanning tunneling microscopy. We suggest that they result from the scattering, by the molecules, of the electrons populating the surface resonance associated with the lowest image potential state of the insulating film on a metal system. These patterns are nearly independent on the thickness of the film from two to five KBr monolayers, implying that they are localized near the surface of the insulating film. The electrons exhibit a parabolic dispersion relation which yields an effective mass $m^* = 0.62 \pm 0.2\, m_e$.

DOI: 10.1103/PhysRevB.99.035410

I. INTRODUCTION

Electron standing wave (SW) patterns have been repeatedly observed on the (111) planes of noble crystals by scanning tunneling microscopy (STM) and spectroscopy (STS). They result from the scattering of the electrons populating the Shockley-type surface state that is present on these surfaces by defects such as steps [1,2], atoms [3] or molecules [4]. These SW patterns have been studied in great detail, providing useful information on the dispersion relation [1,2] and dynamics [5] of the electrons in these states. The direct imaging of the Fermi surface contour on a metal surface by STM was demonstrated by calculating the power spectrum of the constant current image of the pattern generated by a random distribution of point-like surface defects [6]. This finding gave birth to the "Fourier transform-STM" technique, which has strongly contributed to the understanding of the electronic structure of high-temperature (high-T_c) superconductors [7].

More recently, these techniques have been used to study the two-dimensional (2D) electron gas associated with the field emission resonances (FER) [8–10], which are accessible by STM and STS by monitoring constant current $Z(V)$ spectra and their derivative dZ/dV [11–13]. In the absence of any applied electric field, electrons can be trapped near the surface in image potential states (IPS), which are formed by the interaction of the electron with its image charge in the substrate [8]. When the surface is investigated by STM, the applied electric field causes a Stark shift, and these states evolve continuously toward the geometric resonance spectrum associated with the triangular potential created by the substrate and the field [13], as investigated by Gundlach [14].

In this paper, we report on the STM observation of SW patterns around single hexa-*peri*-hexabenzocoronene (HBC) molecules [inset in Fig. 1(a)] adsorbed on the surface of thin KBr(001) films grown on Ag(111). We suggest that these patterns correspond to standing waves formed by the scattering of the electrons populating the lowest energy FER of the system by the molecules. We demonstrate that the 2D electron gas associated with this FER is localized near the surface of the insulating film. Finally, we extract the electron dispersion relation and discuss the specificity of the molecule as an electron scattering center.

II. EXPERIMENTAL METHODS

The experiments are performed in a UHV system including a preparation chamber and a low temperature (5K) STM from Scienta Omicron equipped with SPECS control electronics. All images and spectra are recorded at a temperature of 5 K with platinum STM tips. The Ag(111) sample is cleaned by repeated Ar^+ sputtering followed by annealing at 750 K. KBr is evaporated from a tantalum crucible onto the substrate at room temperature. HBC molecules are deposited from a heated crucible directly onto the cold substrate ($<$10 K) in the microscope.

III. RESULTS

A dZ/dV spectrum recorded on two monolayers (MLs) of KBr is displayed in Fig. 1(c). The peak appearing at $V_S = 2.9$ V (FER-1) is associated with the first FER of the KBr/Ag(111) substrate. The spectrum measured above the center of HBC exhibits two additional peaks. As demonstrated in our recent work [15], the peak near 1.5V (MER-1) corresponds to a molecular electronic resonance associated with the lowest unoccupied molecular orbital (LUMO) of HBC. The second peak in Fig. 1(c), near 2.6 V (MER-2), is also attributed to a molecular electronic resonance. No attempt is made to relate it to a single specific molecular orbital as this is generally not possible for higher order resonances [16]. The third peak in Fig. 1(c) (FER-1) corresponds to the first FER of KBr, perturbed by the presence of the molecule.

Constant current topographic images are recorded on a single HBC molecule adsorbed on a KBr bilayer with bias voltage ranging from 2.95 to 3.5 V by steps of 50 mV, i.e., above the FER-1 peak. Some of them are shown in

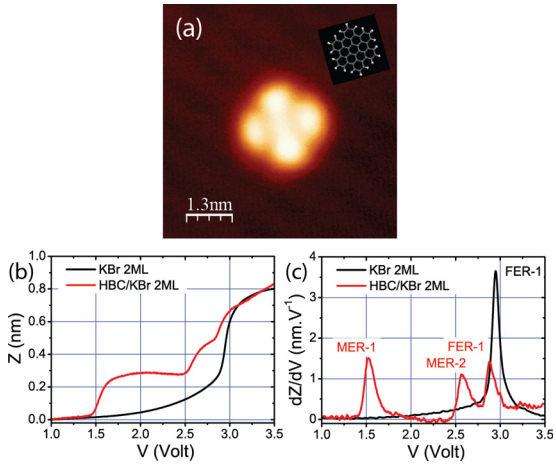

FIG. 1. (a) Constant current STM image of HBC/KBr(2 ML)/Ag(111). $I = 1$ pA, $V = 1.5$ V. Inset: HBC structure. (b) $Z(V)$ and (c) dZ/dV spectra recorded on KBr (black) and HBC (red). $I = 1$ pA.

Fig. 2. The donut-shaped image of the molecule has a diameter and a height that decrease from 3.2 nm and 86 pm [Fig. 2(a)] to 2.4 nm and 61 pm [Fig. 2(d)], respectively, when the bias voltage is increased from 3.05 to 3.5 V. This central feature is surrounded by quasicircular rings, the radial wavelength of which decreases with increasing bias voltage. The amplitude of these rings is of the order of a few pm.

The similarity of these patterns with dI/dV images of surface state SW on metals [1,2] suggests that they correspond to standing waves in the 2D electron gas associated with the 2.9-V field emission resonance (FER-1).

Next, we investigate the influence of the thickness of the KBr film on these SW patterns. Fig. 3 shows constant current dZ/dV spectra measured on Ag(111) and on KBr films of thickness ranging from 2 to 5 ML.

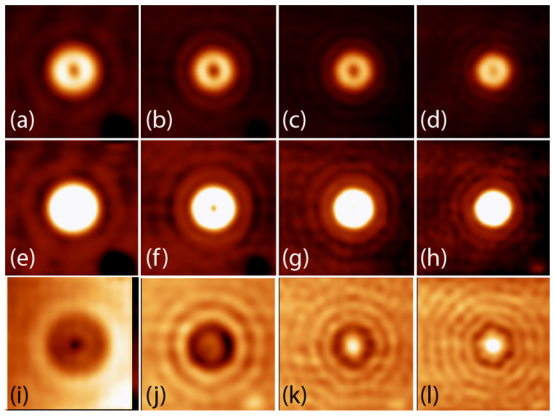

FIG. 2. Constant current topographic STM images on HBC/KBr(2 ML)/Ag(111) with $I = 1$ pA and $V = 3.05$ V [(a) and (e)], 3.2 V [(b) and (f)], 3.35 V [(c) and (g)], 3.5 V [(d) and (h)]. Images (e)–(h) are images (a)–(d) with an enhanced contrast ($\Delta Z = 30$ pm). Images (i)–(l) are image differences: (i) 3.05–3 V, (j) 3.2–3.15 V, (k) 3.35–3.3 V, and (l) 3.5–3.45 V. The size of all the images is 10 × 10 nm.

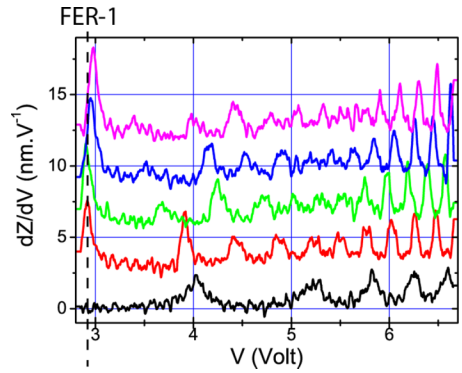

FIG. 3. Constant current dZ/dV spectra on Ag(111) (black) and on KBr films on Ag(111). Red: 2 ML, green: 3 ML, blue: 4 ML, and magenta: 5 ML. $I = 1$ pA. The vertical dotted line is drawn to help visualizing the shift of the FER-1 peak.

As the thickness of the insulating film increases, the characteristic bias voltage of the dZ/dV peaks decreases, except for the first resonance, near 3 V. This behavior derives from the increase of the width of the potential well that supports the resonances when the film thickness increases. The peculiar evolution of the first peak (FER-1), which upshifts by approximately 50 mV from 2 to 5 ML, is discussed in the following.

The topographic images displayed in Fig. 4(a)–4(d) are recorded with $I = 1$ pA and $V = 3.1$ V on HBC on a KBr film with a thickness varying from 2 to 5 ML. Rings are observed in all the images, with a size that slightly increases with the film thickness. This trend can be related to the upward shift of FER-1 observed in Fig. 3. Since this peak shifts by ∼50 mV between 2 and 5 ML, the image on 5 ML at 3.1 V [Fig. 4(d)] is comparable to the image on 2 ML at 3.05 V [Fig. 4(e)]. Indeed, the size of the SW pattern is identical in both conditions as highlighted by the black circles. In addition, the height of the rings is not attenuated when the film thickness increases, in contrast to what would be expected if the electron gas were localized at the metal-insulating film interface. This invariance of the interference pattern with the insulating film

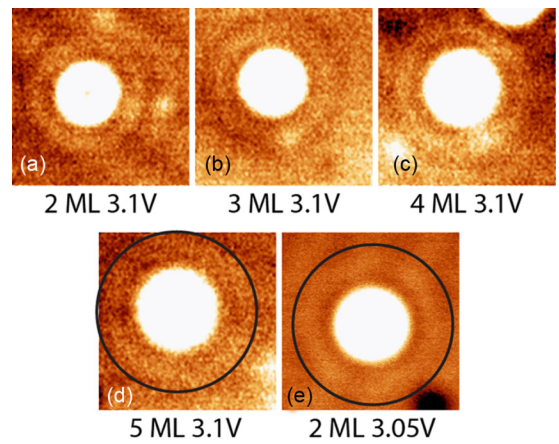

FIG. 4. Constant current topographic STM images of HBC on different thickness of KBr with $I = 1$ pA and (a)–(d) $V = 3.1$ V, and (e) $V = 3.05$ V. Images size: 9.6 × 9. 6nm. The Z scale spans 30 pm for all the images.

thickness strongly suggests that the electron gas that supports the SW does not depend on the metal-insulator interface and consequently is localized near its free surface.

Extracting a dispersion relation from the evolution of the images as a function of the bias is relatively straightforward for SW associated with a surface state on a metal [1,2], but this is not the case for the electrons of the FER-1 for several reasons:

(1) The dispersion relation is usually deduced from the evolution of dI/dV profiles with the bias voltage, when they are recorded with a lock-in amplifier at constant height. This method requires a high tunneling current to get a reasonable signal-to-noise ratio and is therefore difficult to implement on insulating thin films where only very low current can be used. An alternative approach consists of calculating image differences from a set of images measured at small bias voltage intervals. This procedure was applied to the images of Figs. 2(a)–2(d), resulting in Figs. 2(i)–2(l). These image differences are close to dZ/dV images since the images of Fig. 2 are constant current topographic images. But the voltage increment of 50 mV is small enough to consider the $I(Z)$ characteristics as locally linear, making them proportional to dI/dV images. A numerical calculation of the current, based on the Simmons formulation [17], is presented in the Supplemental Material (SM1) [18] . It demonstrates in a simple case that the dispersion relation extracted from this type of image difference is close to the exact one.

(2) The potential well that supports the FER depends on Z and V, which are given by the $Z(V)$ spectra of Fig. 1(b) for a constant current of 1pA. This implies that the energy of this resonance does not stay at qV_S, the energy of the corresponding dZ/dV peak, when the bias voltage V is increased above the resonance, but that it changes according to the $Z(V)$ curve. The energy of the electron injected in the FER deviates from the $q(V - V_S)$ scale in a way that is difficult to predict. Fortunately, numerical calculations [19] show that the deviations from the apparent scale are limited to $+/-10$ meV at most.

(3) Due to the finite radius of curvature of the tip, the electric field above the surface possesses a finite radial component, which repels laterally and accelerates the electrons, resulting in a broadened electron wave vector distribution [10]. This effect is negligible at low bias, when measuring surface state SW patterns on metals [1,2], but becomes significant at the higher bias associated with FERs [10]. The image of the SW pattern on the insulating film is thus expected to deviate from perfect periodicity, the spacing between successive rings decreasing with the distance from the defect. But under the tip, the lateral electric field vanishes as it changes sign from one side to the other along a radius. The effect is then minimal for the first rings and remains small at the scale of our images (10 nm).

The change Δ in the local density of states due to a point scatterer is given by [1]

$$\Delta(E,\rho) \propto \frac{1}{k\rho}\left[\cos^2\left(k\rho - \frac{\pi}{4} + \delta\right) - \cos^2\left(k\rho - \frac{\pi}{4}\right)\right],$$

where E is the energy of the electron measured from the FER band edge and k is its wave vector. ρ is the distance from the center of the scatterer and δ is the phase shift due to the scattering of the electron by the molecule. This expression corresponds to a periodic ring pattern centered on the molecule, as observed in Fig. 2. The radial period is $\pi/k = \lambda/2$, where λ is the wavelength of the electron. We have measured the distance between the first and the second radial minima for the sequence of image differences corresponding to Fig. 2, avoiding the central part of the diagram that is deformed by the topographic image of the molecule. When the second minimum was not visible in the image as is the case at 2.95, 3, and 3.05 V, we consider that the radius of the first radial minimum gives $\lambda/2$, by extrapolating from the images at higher voltage (3.1, 3.15, and 3.2 V) where this is true within a few percent.

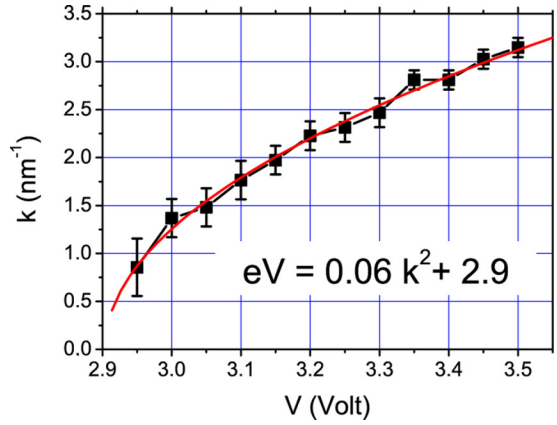

FIG. 5. Dispersion relation extracted from a series of images in the [2.95–3.5 V] bias voltage range, by steps of 50 mV. The red curve is the parabolic fit corresponding to the displayed equation.

The dispersion relation is shown in Fig. 5. It can be fitted with a parabola with $E(k = 0)/q = 2.9$V, in good agreement with the position of the FER-1 peak in Fig. 1(c). The concavity of 0.06 eV nm^2 corresponds to an electron effective mass $m^* = 0.62 \pm 0.2\, m_e$. This m^* value is close to the value of the effective mass in the conduction band of KBr ($0.5\, m_e$) [20] and is comparable to the values measured on thin NaCl films on Cu(111) by time-resolved two-photon photoemission ($0.8 \pm 0.1\, m_e$) [21].

IV. DISCUSSION

First we discuss the possible origins of the confinement of the SW electrons near the free KBr surface. The energy position of the KBr film conduction band (CB) on Ag(111) is not known. A rough estimate can be made from dZ/dV spectra recorded on a KBr bilayer, where a strong modulation of the amplitude of the peaks as a function of the bias voltage can be related to the position of the quantized electronic levels in the insulating layer [22]. This estimation, detailed in SM2 [18], is based on the method presented in Ref. [23]. It suggests that the bottom of the conduction band would be at 3.5 eV above the Fermi level, that is, just above the electronic states contributing to the SW patterns. But what matters for the confinement of the wave function in the vacuum region is not so much the energy of the CB minimum but the energy E_1 of the first quantized state of the insulating film. Below this energy, the electron wave function is exponentially

attenuated in the film: The first quantized level in the insulating layer behaves as an *effective* CB minimum. According to the calculation presented in SM2 [18], E_1 (referred to the CB minimum) decreases from 1.5 V for 2 ML to 0.24 V for 5 ML. The SW states are then separated by at least 0.24 eV from the *effective* CB minimum. This energy separation explains the SW electrons confinement.

Note, however, that this confinement is much weaker than for SW patterns related to Shockley states on metals. Due to the high energy of the electrons, their wave function penetrate the insulating layer giving them an insulator "conduction band" character. This observation could explain why m^* is closer to the effective mass in the CB than in the case of Shockley surface states on metal surfaces.

Our system, KBr/Ag(111), bears strong similarities with the system NaCl/Cu(111) studied by Dıaz-Tendero *et al.* [24]: Ag(111), as Cu(111), shows a surface projected bandgap, NaCl and KBr have the same structure and similar bulk band gaps ($E_{\mathrm{NaCl}} = 8.75\,\mathrm{eV}$, $E_{\mathrm{KBr}} = 8\,\mathrm{eV}$ [19,20]). In addition, the lowering of the work function of the metallic substrate upon the adsorption of a bilayer of the insulating material is of the same order of magnitude for both systems: 1 eV for NaCl/Cu(111), as reported in Ref. [25], and 0.7 eV for KBr/Ag(111) as indicated by the *nc*-AFM $\Delta f(V)$ spectra discussed in SM3 [17,18]. The Ag(111) work function is 4.53 eV [26].

The theoretical study performed by Dıaz-Tendero *et al.* [24] on NaCl/Cu(111) (one to four NaCl layers) demonstrates that the lowest lying excited state is repelled into vacuum by the NaCl film, the electronic density exhibiting a peak that follows the surface of the film. In contrast, the following two higher states have a mixed character in which the image potential state couples with a quantized state of the insulating film conduction band. The electronic density holds then a significant contribution in the film. The position of the first state is also reported to upshifts by ∼100 mV from 2 to 4 ML, while the two others shift downward. We believe that because of this similarity between NaCl/Cu(111) and KBr/Ag(111), the resonances observed on the dZ/dV spectra of Fig. 3 correspond to the states described above, Stark-shifted by the electric field in the tunneling junction. We conclude that FER-1 can be associated with the lowest-lying excited state calculated by Dıaz-Tendero *et al.* [24], meaning that the electron gas and consequently, the SW are located near the free surface of the KBr film, confirming the analysis of Fig. 4 and the previous discussion. This localization obviously favors the interaction between the electron gas of the FER-1 and the molecule.

We have observed that other defects, such as the border of 2-ML high KBr islands on Ag(111) or HBC molecular fragments, also produce SW patterns but they are generally much weaker. The MER-2 molecular peak at 2.6 V is close to the FER-1 resonance at 2.9 V [Fig. 1(c)]. We suggest that this proximity enhances the interaction between the electron gas and the molecule. It is indeed well known from studies of scattering of electron beams by molecules in the gas phase [27] or adsorbed on surfaces [28–30] that the interaction cross section is maximal when the beam energy coincides with the energy of a molecular resonance.

V. CONCLUSION

In summary, we have observed by LT-STM standing wave patterns around single HBC molecules adsorbed at the surface of thin KBr films (2–5 ML) grown on Ag(111). We demonstrate that this phenomenon is related to the presence of an electron gas confined near the free surface of the film. We suggest, on the basis of our experimental results, that these SW patterns are produced by the scattering of the electrons that populates the first Stark-shifted image potential state at the KBr surface.

Further developments could include the study of the dynamical properties of these electrons such as their phase relaxation length and their lifetime by using the methods developed, for instance, in Ref. [5]. More generally, these studies will contribute to increase our understanding of the properties of these thin insulating films of varying thickness, which play a major role in the domain of molecular electronics to decouple atoms or molecules from the supporting metal substrate, as for instance demonstrated recently in Ref. [31].

ACKNOWLEDGMENTS

T.A. acknowledges the French Ministry of Higher Education and Research for a Ph.D. fellowship. C.J.V. acknowledges the financial support of PAPIIT IN114317 UNAM. The images have been processed with the WSXM software [32].

[1] M.F. Crommie, C.P. Lutz, and D. M. Eigler, Imaging standing wave in a two-dimensional electron gas, Nature (London) **363**, 524 (1993).

[2] Y. Hasegawa and Ph. Avouris, Direct Observation of Standing Wave Formation at Surface Steps Using Scanning Tunneling Spectroscopy, Phys. Rev. Lett. **71**, 1071 (1993).

[3] M. F. Crommie, C. P. Lutz, and D. M. Eigler, Confinement of electrons to quantum corrals on a metal surface, Science **262**, 218 (1993).

[4] L. Gross, F. Moresco, L. Savio, A. Gourdon, C. Joachim, and K.-H. Rieder, Scattering of Surface State Electrons at Large Organic Molecules, Phys. Rev. Lett. **93**, 056103 (2004).

[5] L. Bürgi, O. Jeandupeux, H. Brune, and K. Kern, Probing Hot-Electron Dynamics at Surfaces with a Cold Scanning Tunneling Microscope, Phys. Rev. Lett. **82**, 4516 (1999).

[6] L. Petersen, Ph. Hofmann, E. W. Plummer, and F. Besenbacher, Fourier transform–STM: Determining the surface Fermi contour, J. Electron Spectrosc. Relat. Phenom. **109**, 97 (2000).

[7] K. McElroy, R. W. Simmonds, J. E. Hoffman, D. H. Lee, J. Orenstein, H. Elsaki, S. Uchida, and J. C. Davis, Relating atomic-scale electronic phenomena to wave-like quasiparticle states in superconducting $Bi_2Sr_2CaCu_2O_{8+\delta}$, Nature **422**, 592 (2003).

[8] P. Wahl, M. A. Schneider, L. Diekhöner, R. Vogelgesang, and K. Kern, Quantum Coherence of Image-Potential States, Phys. Rev. Lett. **91**, 106802 (2003).

[9] S. Stepanow, A. Mugarza, G. Ceballos, P. Gambardella, I. Aldazabal, A. G. Borisov, and A. Arnau, Localization, splitting, and mixing of field emission resonances induced by alkali metal clusters on Cu(100), Phys. Rev. B **83**, 115101 (2011).

[10] J. I. Pascual, C. Corriol, G. Ceballos, I. Aldazabal, H.-P. Rust, K. Horn, J. M. Pitarke, P. M. Echenique, and A. Arnau, Role of the electric field in surface electron dynamics above the vacuum level, Phys. Rev. B **75**, 165326 (2007).

[11] G. Binnig and H. Rohrer, Scanning tunneling microscopy, Helv. Phys. Acta **55**, 726 (1982).

[12] R. S. Becker, J. A. Golovchenko, and B. S. Swartzentruber, Electron Interferometry at Crystal Surfaces, Phys. Rev. Lett. **55**, 987 (1985).

[13] G. Binnig, K. H. Frank, H. Fuchs, N. Garcia, B. Reihl, H. Rohrer, F. Salvan, and A. R. Williams, Tunneling Spectroscopy and Inverse Photoemission: Image and Field States, Phys. Rev. Lett. **55**, 991 (1985).

[14] K. H. Gundlach, Zur berechnung des tunnelstroms durch eine trapezförmige potentialstufe, Solid State Electron. **9**, 949 (1966).

[15] T. Ardhuin, O. Guillermet, A. Gourdon, and S. Gauthier, Molecular resonance imaging and manipulation of hexabenzocoronene on NaCl(001) and KBr(001) on Ag(111), J. Phys. Chem. C, **122**, 11905 (2018).

[16] W.-H. Soe, H. S. Wong, C. Manzano, M. Grisolia, M. Hliwa, X. Feng, K. Müllen, and C. Joachim, Mapping the excited states of single hexa-peri-benzocoronene oligomers, ACS Nano **6**, 3230 (2012).

[17] J. G. Simmons, Generalized formula for the electric tunnel Effect between similar electrodes separated by a thin insulating film, J. Appl. Phys. **34**, 1793 (1963).

[18] See Supplemental Material at http://link.aps.org/supplemental/10.1103/PhysRevB.99.035410 for estimations of (1) the dispersion relation from a model calculation, (2) the position of the KBr conduction band minimum for a bilayer on Ag(111) and (3) the change in the work function upon adsorption of a KBr bilayer on Ag(111).

[19] T. Ardhuin, O. Guillermet, and S. Gauthier (unpublished).

[20] L. J. Page and E. H. Hygh, Calculation of energy bands in alkali halides, Phys. Rev. B **1**, 3472 (1970).

[21] M. Muntwiler and X.-Y. Zhu, Formation of Two-Dimensional Polarons that are Absent in Three-Dimensional Crystals, Phys. Rev. Lett. **98**, 246801 (2007).

[22] T. Ardhuin, Etude par STM et NC-AFM des mécanismes de charge de molécules individuelles sur substrats isolants, Ph.D. thesis, Université Toulouse 3 Paul Sabatier, 2018.

[23] Y. R. Wang, J. A. Kubby, and W. J. Greene, Thin film electron interferometry, Mod. Phys. Lett. **5**, 1387 (1991).

[24] S. Dıaz-Tendero, A. G. Borisov, and J.-P. Gauyacq, Theoretical study of the electronic excited states in ultrathin ionic layers supported on metal surfaces: NaCl/Cu(111), Phys. Rev. B **83**, 115453 (2011).

[25] R. Bennewitz, M. Bammerlin, M. Guggisberg, C. Loppacher, A. Baratoff, E. Meyer, and H.-J. Güntherodt, Aspects of dynamic force microscopy on NaCl/Cu(111): Resolution, tip–sample interactions and cantilever oscillation characteristics, Surf. Interface Anal. **27**, 462 (1999).

[26] G. N. Derry, M. E. Kern, and E. H. Worth, Recommended values of clean metal surface work functions, J. Vac. Sci. Technol. A **33**, 060801 (2015).

[27] G. J. Schulz, Resonances in electron impact on diatomic molecules, Rev. Mod. Phys., **45**, 423 (1973).

[28] J. E. Demuth, D. Schmeisser, and Ph. Avouris, Resonance Scattering of Electrons from N_2, CO, O_2, and H_2 Adsorbed on a Silver Surface, Phys. Rev. Lett. **47**, 1166 (1981).

[29] R. E. Palmer and P. J. Rous, Resonances in electron scattering by molecules on surfaces, Rev. Mod. Phys., **64**, 383 (1992).

[30] P. J. Rous, Theory of negative ion formation at surfaces, Comput. Phys. Commun. **137**, 33 (2001).

[31] W. Steurer, J. Repp, L. Gross, and G. Meyer, Damping by sequentially tunneling electrons, Surf. Sci. **678**, 112 (2018).

[32] I. Horcas, R. Fernandez, J.M. Gomez-Rodriguez, J. Colchero, J. Gomez-Herrero, and A. M. Baro, WSXM: A software for scanning probe microscopy and a tool for nanotechnology, Rev. Sci. Instrum. **78**, 013705 (2007).